Chemical Science

ROYAL SOCIETY OF CHEMISTRY

EDGE ARTICLE

View Article Online
View Journal | View Issue

Cite this: *Chem. Sci.*, 2024, **15**, 14399

All publication charges for this article have been paid for by the Royal Society of Chemistry

Received 25th June 2024
Accepted 8th August 2024

DOI: 10.1039/d4sc04179h

rsc.li/chemical-science

Cross-linking enhances the performance of four-electron carbonylpyridinium based polymers for lithium organic batteries†

Hongyan Li, Ling Chen, Fangfang Xing, Hongya Miao, Jing Zeng, Sen Zhang and Xiaoming He *

Design and integration of multiple redox-active organic scaffolds into tailored polymer structures to enhance the specific capacity and cycling life is a long-term research goal. Inspired by nature, we designed and incorporated a 4-electron accepting dicarbonylpyridinium redox motif into linear (**DBMP**) and cross-linked polymer (**TBMP**) structures. Benefiting from the suppressed solubility and higher electronic conductivity, the cross-linked **TBMP** based electrode exhibits improved cycling stability and higher specific capacity than the linear counterpart. After 4000 cycles at 1 A g^{-1}, **TBMP** can maintain a high capacity of 252 mA h g^{-1}, surpassing the performance of many reported organic cathodes. The structural evolution and reaction kinetics during charge and discharge have been investigated in detail. This study demonstrates that cross-linking is an effective strategy to push the bio-derived carbonylpyridinium materials for high performance LOBs.

Introduction

Rapid advances in rechargeable lithium-ion batteries (LIBs) have revolutionized the portable electronics and electric vehicle markets.[1,2] State-of-the-art LIB cathode materials based on transition metal oxides are reaching their theoretical limits, and there is little room for further improvement. In addition, the limited and unevenly distributed mineral resources and ever-increasing prices restrict the further large-scale application in LIBs. In this context, organic materials are promising candidates for next-generation battery systems in view of their structural diversity and tailored electrochemical properties.[3–6] Thanks to great efforts, various building blocks, including free radicals,[7–9] azobenzenes,[10–12] imines,[13,14] conjugated carbonyl groups[15–18] and viologens,[19–23] have been successfully utilized as redox-active units to construct organic electrodes. However, the charge storage capacity is restricted to either one or two electrons per molecule or unit. Therefore, the development of novel molecular skeletons that can reversibly accept multiple electrons is highly desirable to afford high energy density and overall capacity; however, it is very challenging and rarely reported.[24–26]

Over billions of years of natural selection, nature has evolved excellent energy storage and transportation systems, which offer researchers tremendous inspiration for the design of high-performance electrode materials. Recent advances have shown that chemical engineering of active moieties in biological systems is a promising approach to design high-performance organic electrodes for lithium organic batteries (LOBs), due to the already built-in functionality.[27] For instance, Seferos and coworkers reported a non-conjugated polymer pendant redox-active flavin (vitamin B2) moiety as the cathode for Li-ion batteries.[28] Inspired by the naturally occurring NAD^+/NADH couple, we recently developed a series of carbonylpyridinium based key motifs that can reversibly accept multiple electrons for battery applications.[19,29–31] In order to realize long cycling life without obvious capacity decay, one basic requirement is to suppress the solubility of organics in electrolytes. A solution to this issue is introducing polymer structures. In particular, for pyridinium-based redox centers, one simple strategy is polycondensation *via* the Menshutkin reaction of bi-pyridine precursors with α,α′-dibromo-*p*-xylene to form linear polycationic polymers. However, the poor solubility of polycationic polymers in common organic solvents causes precipitation during the polymerization step, and most of the reported polymers have relatively low molecular weights (about 4–12 repeat units),[20,22,32] which cannot fully satisfy the long cycling stability. It is proposed that tailoring the polymer structures from linear to cross-linked architecture can effectively address the above issue.[33]

In this work, we examined two carbonylpyridinium-based non-conjugated polymers, linear **DBMP** and cross-linked **TBMP**, as cathodes for lithium organic batteries. Both polymers have the same phenyl-bridged dicarbonylpyridinium

Key Laboratory of Applied Surface and Colloid Chemistry (Ministry of Education), School of Chemistry and Chemical Engineering, Shaanxi Normal University, Xi'an 710119, P.R. China. E-mail: xmhe@snnu.edu.cn

† Electronic supplementary information (ESI) available. See DOI: https://doi.org/10.1039/d4sc04179h

redox unit that can accept four electrons. Our results reveal that the cross-linked **TBMP** based electrode has improved cycling stability and higher specific capacity than the linear counterpart, not only because of the suppressed solubility but also due to higher electronic conductivity. Benefiting from the joint contribution of both the skeleton and redox-active counter Br^- anions, **TBMP** delivers a high capacity of 252 mA h g^{-1} after 4000 cycles at 1 A g^{-1}. Its performance ranks at the top among all reported pyridinium-based LOB electrodes. This work is a major advancement to push the bio-derived carbonylpyridinium materials for high performance LOBs.

Results and discussion

Aryl-bridged di-carbonylpyridinium systems have been previously demonstrated by us to be capable of reversibly storing four electrons.[30] In this study, to maximize the theoretical capacity (C_{theor}), we shortened the aryl linkers (*e.g.* biphenyl and bithiophene) to a phenyl moiety. Toward this goal, a key intermediate, 1,4-phenylenebis(4-pyridylmethanone) (**M1**) was prepared according to the literature.[34] From **M1**, linear polymer **DBMP** and cross-linked analogue **TBMP** can be facilely synthesized in excellent yields (>80%) *via* the Menshutkin reaction by polycondensation with α,α′-dibromo-*p*-xylene (**S1**) or 1,3,5-tris(bromomethyl)benzene (**S2**) in dry DMF at 90 °C. In addition, a model compound **M2** was also prepared, in order to provide a fundamental understanding of the structural and electrochemical properties of polymers. Detailed preparation and characterization are presented in the ESI (Fig. S1–S7†).

The structure of **M2** was confirmed by conventional techniques (^{1}H and ^{13}C NMR and MS). Because of the limited solubility of the two polymers **DBMP** and **TBMP** in common organic solvents, their structures were characterized by FT-IR and solid-state ^{13}C NMR (Fig. 1). Similar to the model compound **M2**, the two polymers displayed characteristic C=O and C=N stretching peaks at 1672 and 1564 cm^{-1}, confirming that carbonylpyridinium redox centers are well preserved in the polymers (Fig. 1a and S8†). Meanwhile, the characteristic C–Br (652–661 cm^{-1}) from the two brominated starting materials (**S1** and **S2**) nearly disappeared, further confirming the successful polymerization. As shown in the solid state ^{13}C NMR spectrum (Fig. 1b), **DBMP** and **TBMP** exhibited characteristic C=O carbon signals at 220–180 ppm and $CH_2(N^+)$ signals at 50–70 ppm. Several other peaks in the range of 160–110 ppm can be well assigned to other aromatic carbons. These ^{13}C NMR peaks can be well compared to those of **M2**. Based on the proton NMR, the degree of polymerization (DP) was determined to be 13 (detailed method is in ESI, Fig. S7†).

Distinct morphologies were observed for the two polymers by scanning electron microscopy (SEM). As shown in Fig. 1c and d, cross-linked **TBMP** exhibits severe aggregation of spherical particles with a diameter of 2–5 μm, while linear **DBMP** consists of irregular bulky morphology with comparable size. The powder X-ray diffraction (PXRD) patterns of the two polymers display a broad peak in the range of 20–30° (Fig. S9†), implying their amorphous nature in the solid state. The two polymers have good thermal stability, with the decomposition temperatures determined to be 180 and 200 °C for **DBMP** and **TBMP**, respectively (Fig. S10†).

Interestingly, the as-prepared solids of **M2**, **DBMP** and **TBMP** display pale-yellow, brown and reddish brown colors, respectively (Scheme 1), indicating their different energy band gaps. To characterize their optical properties, UV-vis experiments were performed (Fig. 1e). DMF solution of **M2** is colorless and exhibits an intense absorption peak at 279 nm, belonging to the π–π* transition. Compared to its solution state, solid-state **M2** shows an obvious red shift and has broad absorption in the visible region of 300–600 nm, which was tentatively attributed

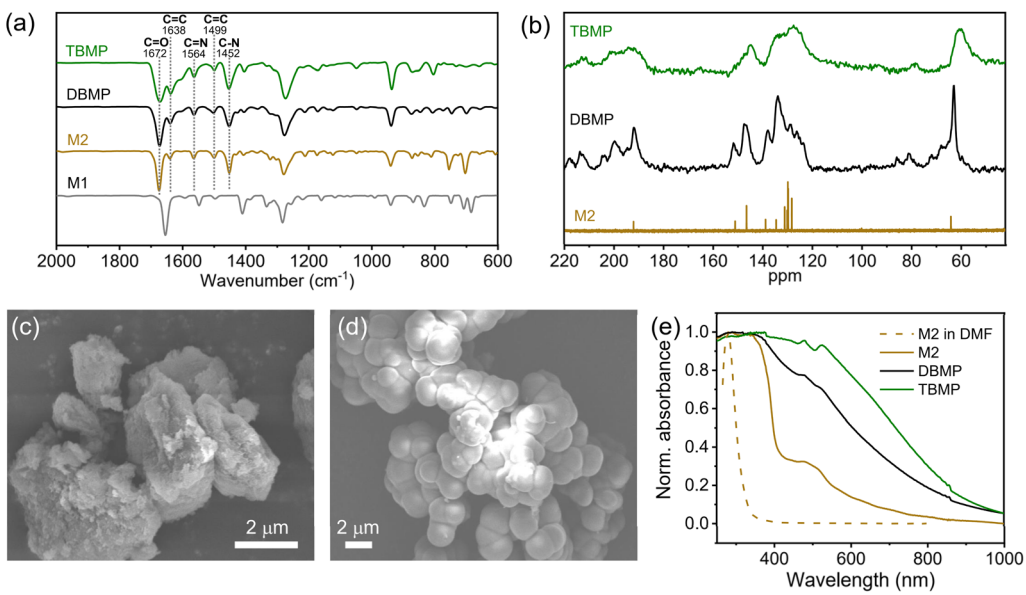

Fig. 1 Characterization of **M2**, **DBMP** and **TBMP**. (a) FT-IR spectra, (b) solid-state ^{13}C NMR spectra, (c) SEM image of **DBMP**, (d) SEM image of **TBMP**, and (e) UV-vis spectra of **M2**, **DBMP** and **TBMP** in the solid state (solid lines) and **M2** in DMF solution (dashed line).

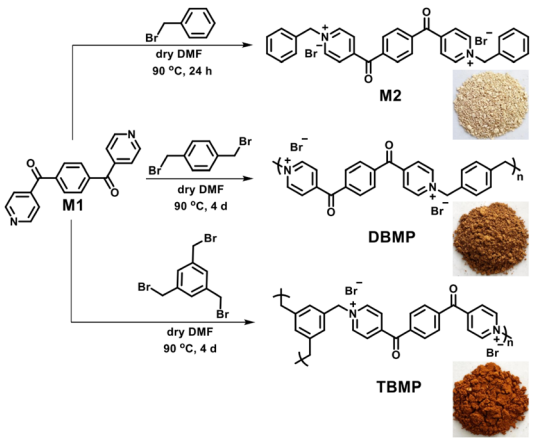

Scheme 1 Synthetic route of the target compounds.

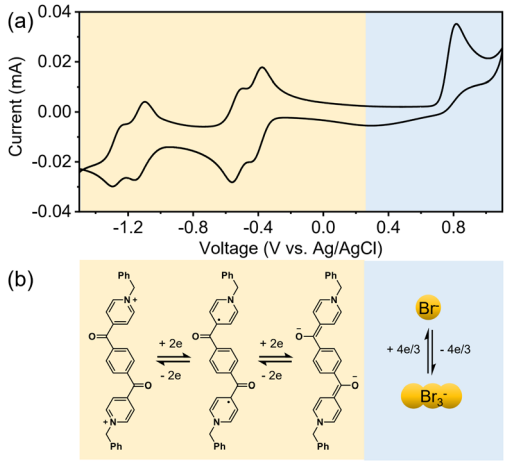

Fig. 2 Electrochemistry of **M2**. (a) CV of **M2** in DMF solution ($c = 1$ mM) with 0.1 M $TBAPF_6$ as the electrolyte. (b) Reversible redox processes of carbonypyridinium and Br^-.

to the donor–acceptor (D–A) charge transfer from electron-rich Br^- to the electron-deficient carbonylpyridinium skeleton.[35] Due to the close proximity of positive redox units in the polymer, the electron-accepting properties of carbonylpyridinium would be enhanced, leading to further red shift from **M2**, through **DBMP**, to **TBMP**. From Tauc plots (Fig. S11†), the calculated optical bandgaps (E_g) were found to follow the trend of **M2** (2.20 eV) < **DBMP** (1.94 eV) < **TBMP** (1.61 eV). The apparent narrowest E_g of is beneficial to facilitate the electron transportation, which is confirmed by its higher electronic conductivity (*vide infra*).

Before investigating the electrochemistry of the two polymers, the electrochemistry of model compound **M2** was initially evaluated by cyclic voltammetry (CV). As shown in Fig. 2a, both the Br^- anion and carbonylpyridinium skeleton are redox active. The irreversible peak at a higher potential of 0.8 V (*vs.* Ag/AgCl) is assigned to the Br^-/Br_3^- redox couple. The carbonylpyridinium skeleton displays four reversible redox pairs at a lower potential range from −0.2 to −1.4 V (*vs.* Ag/AgCl), with the reduction potentials determined to be $E_{1/2}(1) = -0.38$ V, $E_{1/2}(2) = -0.50$ V, $E_{1/2}(3) = -1.13$ V, and $E_{1/2}(4) = -1.25$ V. Fig. 2b depicts the multiple electron transfer processes of **M2**. For the positive skeleton of **M2**, the first two electron uptake leads to the formation of neutral radical species, and the second two-electron reduction leads to the formation of anionic species. The differential pulse voltammogram (DPV) of **M2** further confirms the multistep reduction processes of **M2** (Fig. S12†), and the pattern is consistent with the CV. These results suggest that the two carbonylpyridinium units in **M2** are not independent; they affect each other as a result of the conjugation effect. The voltage separation between two redox events is approximately 0.74 V, comparable to a previous report. The electrochemical stability of **M2** was also examined. As shown in Fig. S13,† all the multiple redox signals of **M2** can retain very well at various scanning speeds from 50 mV s^{-1} to 1000 mV s^{-1}, implying excellent electrochemical reversibility. According to the Randles–Sevcik equation,[36] the diffusion coefficient was calculated to be 1.2–2.3 × 10^{-7} cm^2 s^{-1}, by fitting the linear plot of the peak current *vs.* the square root of the scan rate.

Based on the electrochemistry of **M2**, it is reasonable to conclude that each carbonylpyridinium redox center in polymers **DBMP** and **TBMP** could reversibly take up four electrons. In addition, by including the contribution of redox-active counter Br^- anions, each repeat unit of **DBMP** and **TBMP** delivers 16/3 electrons and therefore has a theoretical capacity (C_{theor}) of 259 and 272 mA h g^{-1}, respectively.

To study the polymers as cathodes for LOBs, we fabricated a coin-cell half battery by using Li metal as the counter electrode. The working electrode consisted of 40 wt% polymer as the active material, 40 wt% carbon black (ECP-600JD) as the conductive additive, 20 wt% polyvinylidene fluoride (PVDF) binder, and 2.0 M $LiClO_4$ in tetraglyme (G4) as the electrolyte.

The cells were first evaluated by CV over the voltage range of 1.2–3.8 V *vs.* Li/Li^+. As shown in Fig. 3a, both **DBMP** and **TBMP** based cathodes present three reversible pairs of redox peaks. The redox pair at a high potential of 3.47/3.64 V is attributed to the one-step reaction of the Br^-/Br_3^- redox couple, comparable to the reported literature.[23] The other two redox pairs at 2.40/2.59 and 2.06/2.25 V belong to the four-electron uptake of the carbonylpyridinium centers. Note that the voltage separation between two major redox pairs of carbonylpyridinium is *ca.* 0.34 V, which is much smaller than that observed for **M2** in solution (0.74 V). The reason could be tentatively attributed to the space effect of the neighboring positively charged redox center in the polymer backbone, which can facilitate the electron injection.[37,38] The galvanostatic charge–discharge (GCD) tests show that both polymers exhibit three distinct plateaus in both their charge and discharge profiles (Fig. 3b), which agree well with the three couples of redox peaks in the CV curves.

Fig. 3c shows the rate performance of the two polymers. Apparently, the crosslinked polymer exhibited much higher capacities compared with the linear polymer, except for the first few cycles. Specifically, crosslinked **TBMP** exhibited a stable capacity of 190 mA h g^{-1} at 0.2 A g^{-1}, as compared with a capacity of 132 mA h g^{-1} for its linear analogue **DBMP**. During the first 10 cycles at 0.05 A g^{-1}, the delivered capacity of **TBMP** is lower than that of **DBMP**, but the value underwent a rapid

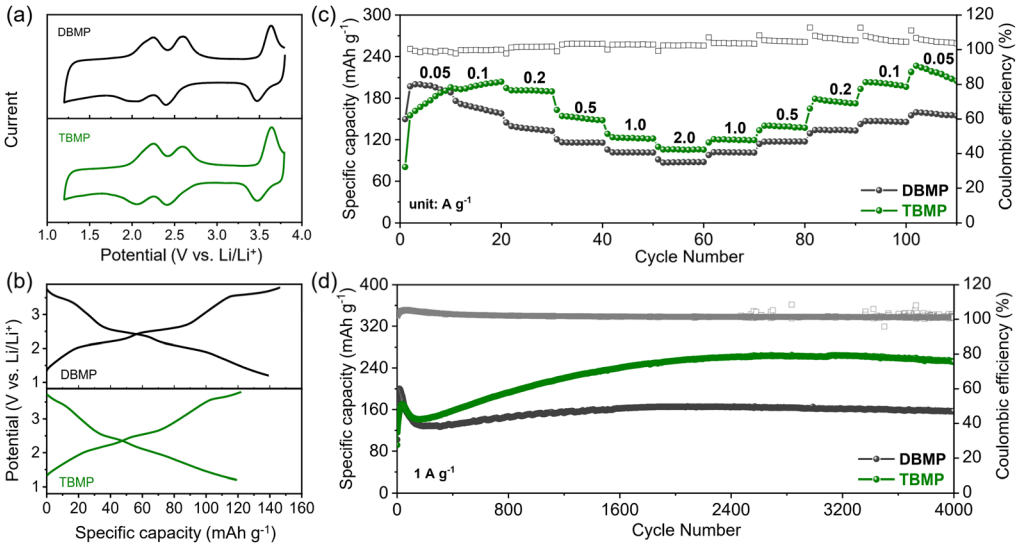

Fig. 3 Electrochemical and battery performance. (a) CV curves of **DBMP** and **TBMP** at 1.0 mV s^{-1}. (b) The GCD curves of **DBMP** and **TBMP** at 1.0 A g^{-1} of the third cycle. (c) Rate performance. (d) Cycling performance and coulombic efficiency at 1.0 A g^{-1}.

increase. The reason is likely because of the gradual swelling process of the crosslinked polymer that could optimize the interfaces with the electrolyte and carbon additive.

In order to evaluate the cycle stability, the batteries were subjected to repeated charge/discharge cycles (Fig. 3d and S14†). Fig. 3d shows the cycling performance at 1 A g^{-1} in the 1.2–3.8 V (*vs.* Li/Li^+) voltage range. Cross-linked **TBMP** exhibits much higher capacities than **DBMP**, except for the initial decades of cycles. In the initial 100 cycles, capacity fluctuation was observed for both **TBMP** and **DBMP**, which was attributed to the formation of the SEI film, the decomposition of the electrolyte and slight solubility of polymers.[29,30] After that, the **TBMP**-based electrode displays gradually increased capacities with a maximum value of 252 mA h g^{-1} after 2000 cycles, and the capacity can be maintained without decay even after 4000 cycles. We attribute this behavior to gradual swelling of its cross-linked structure that can optimize the contact with the electrolyte and carbon additives, leading to more efficient conductive pathways and high utilization of redox centers. Such a behavior has also been observed in other lithium-organic hybrid batteries.[4,19] In contrast, **DBMP** only delivered 157 mA h g^{-1} after 4000 cycles at 1.0 A g^{-1}. The smaller capacity of **DMBP** can be due to the dissolution of the oligomer with a low DP. This was further confirmed by the solubility test (Fig. S15†). After soaking both polymers in G4 electrolyte for 3 days, solution of **DMBP** displayed a light yellow color, along with the appearance of a UV-vis absorption peak at 290 nm. In contrast, the suspended **TMBP** in G4 remained colorless, without detectable UV-vis absorption. All these confirm that **TMBP** can further suppress the solubility.

To better understand the better performance of **TBMP**, the electronic and ionic conductivities of the two polymers were evaluated. The electrical conductivity was determined by the linear sweep voltammetry test with a two-point probe. Fig. 4a shows the *I*–*V* plot of the two polymer pellets. The electrical conductivity (σ) is determined according to the equation $\sigma = L/(RS)$, where R, S and L represent the resistance, surface area and thickness of the pellet.[39] Experimental data confirm that the electrical conductivity of **TBMP** (8.6×10^{-8} S cm^{-1}) is one order of magnitude higher than that of **DBMP** (3.7×10^{-9} S cm^{-1}). The better electrical conductivity of the cross-linked polymer was also confirmed by its lower charge-transport resistance in the electrochemical impedance spectroscopy (EIS) (Fig. S16†), as well as powder conductivity measurement using a four-probe system (Fig. S17†). Such significantly improved electrical conductivity of the cross-linked polymer is consistent with its narrowest band gap, due to the more effective charge transfer as a result of the cross-linking induced space confinement.[35]

The galvanostatic intermittent titration technique (GITT) was used to quantify the ion conductivity (Fig. S18†). As shown in Fig. 4b, the calculated apparent diffusion coefficients (D_{app}) for two polymers are comparably in the order of *ca.* 10^{-10} cm^2 s^{-1}. These values are much higher than many of the reported data for organic electrodes (typically in the level of 10^{-13}–10^{-11} cm^2 s^{-1}),[40–42] which may be because of the unique anion and cation co-transfer of carbonylpyridinium. Overall, the higher

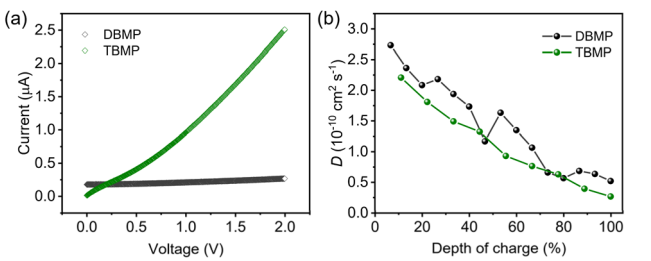

Fig. 4 Ionic and electronic conductivities of **DBMP** and **TBMP**. (a) *I*–*V* plot of **DBMP** and **TBMP** pellets for measuring the electrical conductivity. (b) The ion diffusion coefficient calculated from the GITT profiles of **DBMP** and **TBMP** based electrodes.

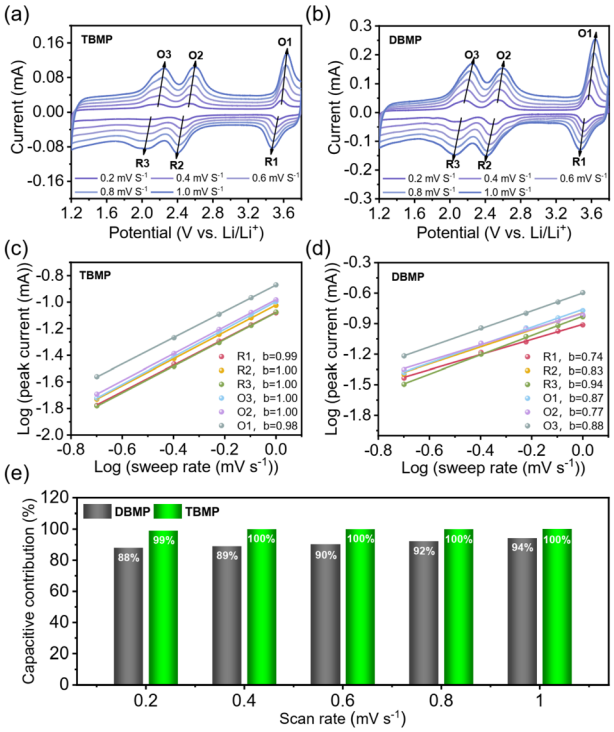

Fig. 5 (a and b) CV curves of (a) **TBMP** and (b) **DBMP** at varying scan rates. (c and d) Plot of log(*i*) *versus* log(*v*) of multiple redox peaks for (c) **TBMP** and (d) **DBMP**. (e) Comparison of the capacitive contribution of **TBMP** and **DBMP** at different scan rates.

electronic and ionic conductivity means fast electron transfer and ion diffusion, which is of great significance for the rate performance of the **TBMP** based electrode.

The in-depth charge storage mechanism of **TBMP** and **DBMP** based cathodes was investigated by CV analysis with various sweep rates (Fig. 5). As can be seen from the CV profiles (Fig. 5a and b), multiple redox pairs at various scan rates were continuously observed, corroborating the electrochemical stability of the polymers. Elevating the sweep rate leads to the gradually increased current response. The capacity contributions can be analyzed using *b* values according to the power law $i = a \times v^b$, where *i* denotes the peak current, *v* signifies the scan rate, *a* is a constant, and *b* is a variable coefficient that denotes different mechanisms.[43,44] Specifically, *b* values of 0.5 and 1 indicate diffusion-controlled and surface-controlled (capacitive) kinetics, respectively. Based on the linear fit of log(*v*) and log(*i*), the *b*-values of multiple redox peaks for cross-linked polymer **TBMP** are close to 1, higher than that for the linear counterpart **DBMP** (0.74–0.94). More accurately, capacitive contributions of **TBMP** and **DBMP** were determined to be 99% and 88% at 0.2 mV s^{-1}. A higher capacitive contribution of **TBMP** further suggests its fast electrochemical kinetics and good rate performance.

The proposed redox mechanism and structural evolution of **TBMP** is illustrated in Fig. 6a. Both carbonylpyridinium units and Br^- anions serve as redox centers. The carbonylpyridinium unit would undergo reversible transformation between three states: cationic species, neutral radical species, and anionic species. This structural evolution is also accompanied by subsequent anion and cation insertion and de-insertion. The redox-active Br^- would oxidize to Br_3^- during charge and reduce back during discharge.

To characterize the above structural evolution, *ex situ* FT-IR, X-ray photoelectron spectroscopy (XPS) and electron paramagnetic resonance (EPR) analysis were performed (Fig. 6b–f). Selected points in the discharge/charge curve for the study are shown in Fig. 6b. FT-IR characterization shows that the peak intensity of C=O and C=N at 1668 and 1564 cm^{-1} was found to be strongly weakened upon discharging to 1.2 V (*vs.* Li^+/Li) (Fig. 6c). The intensity showed a reverse trend during subsequent charge, manifesting the reversible electrochemical process of carbonylpyridinium centers. The structural evolution was also verified by XPS (Fig. 6d and e). Upon discharging, the O 1s signal at 531.5 eV shifted to 532.5 eV, indicating the reduction of C=O to C–O–Li. Moreover, the N 1s peak of C=N at

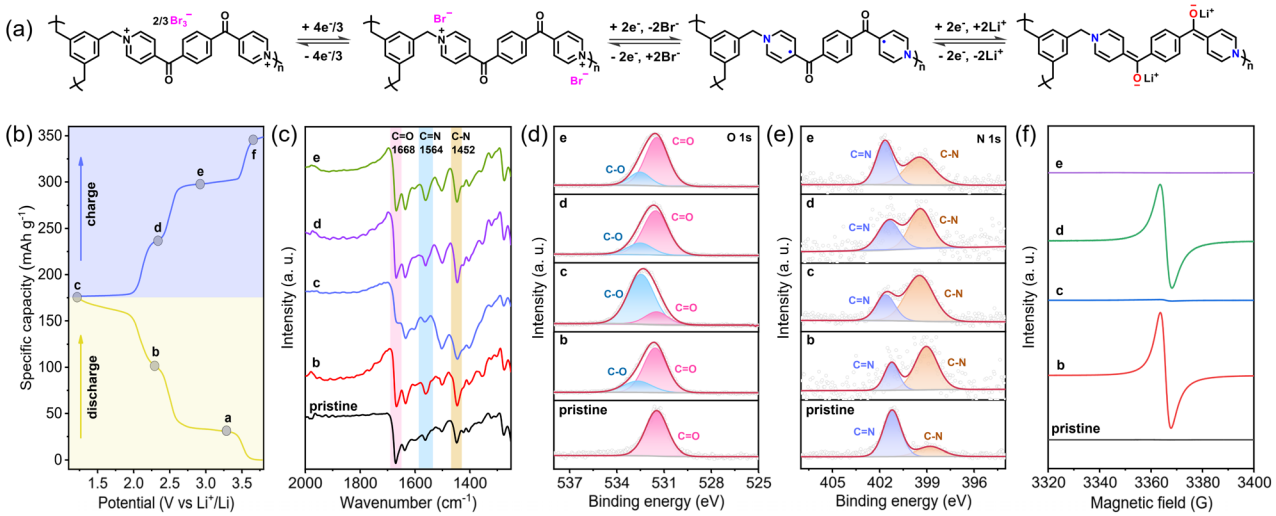

Fig. 6 (a) Proposed redox mechanism and structural evolution of the **TBMP** based electrode. (b) Representative discharge and charge profiles, (c) *ex situ* FT-IR spectra, high-resolution O 1s (d) and N 1s (e) XPS spectra, and (f) EPR spectra of the **TBMP** electrode recorded at marked points in (b).

401.2 eV in the fresh electrode shifted to low binding energy at the 399.5 eV index to C–N. The XPS signals can also be nearly recovered at the fully charged state. To characterize the radical intermediate, the electron paramagnetic resonance (EPR) experiment was performed (Fig. 6f). A strong EPR signal at 3366 G appeared after discharging to 2.2 V and then disappeared after further discharging to 1.2 V. Subsequent recharging to 3.0 V led to a reverse trend, suggesting its reliable reversibility. These results clearly demonstrate the reversible structural evolution of the carbonylpyridinium redox center proposed in Fig. 6a.

The transformation of Br^- to Br_3^- was also confirmed by XPS (Fig. S19a†). In the pristine state, two peaks at 67.5 eV and 66.5 eV can be assigned to Br $3d_{3/2}$ and Br $3d_{5/2}$, respectively. After being charged to 3.8 V, these two peaks shift to a higher binding energy, confirming that Br^- was oxidized to a high valence state.[23] In accord with the XPS spectra, Raman spectra further confirm the oxidation of Br^- to Br_3^-, with the Br_3^- signal observed at 130–170 cm^{-1} after being charged to 3.8 V (Fig. S19b†).

Conclusions

In conclusion, we designed two non-conjugated polymers **DBMP** and **TBMP** and evaluated their electrochemistry as cathodes for LOBs. Owing to the effective ability to suppress dissolution and higher electronic conductivity resulting from the cross-linked structure, **TBMP** exhibited remarkably improved cyclability and rate performance compared with **DBMP**. Even after 4000 cycles at 1.0 A g^{-1}, **TBMP** can deliver a high capacity of 252 mA h g^{-1}, ranking at the top among the reported organic materials for LOBs. This work demonstrates an effective cross-linking approach to boost the battery performance of carbonylpyridinium based polymers. It is believed that such a strategy can be extended to other redox-active modified pyridinium based polymers.

Data availability

The data supporting this article have been included as part of the ESI.†

Author contributions

H. Li synthesized the materials and performed the experiments. L. Chen, F. Xing and H. Miao helped in the discussion of the electrochemical performance. J. Zeng and S. Zhang assisted in electrochemical characterization. X. He supervised the project and prepared the manuscript with input from all the other authors.

Conflicts of interest

There are no conflicts to declare.

Acknowledgements

This work was supported by the Fundamental Research Funds for the Central Universities (GK202201006) and the Innovation Capability Support Program of Shaanxi (No. 2020TD024). X. H. thanks Shaanxi Normal University for the funding support.

Notes and references

1 M. Li, J. Lu, Z. Chen and K. Amine, *Adv. Mater.*, 2018, **30**, 1800561.
2 M. Armand and J. M. Tarascon, *Nature*, 2008, **451**, 652–657.
3 Y. Liang, Z. Tao and J. Chen, *Adv. Energy Mater.*, 2012, **2**, 742–769.
4 T. B. Schon, B. T. McAllister, P.-F. Li and D. S. Seferos, *Chem. Soc. Rev.*, 2016, **45**, 6345–6404.
5 J. Kim, J. H. Kim and K. Ariga, *Joule*, 2017, **1**, 739–768.
6 S. Lee, G. Kwon, K. Ku, K. Yoon, S.-K. Jung, H.-D. Lim and K. Kang, *Adv. Mater.*, 2018, **30**, 1704682.
7 K. Nakahara, S. Iwasa, M. Satoh, Y. Morioka, J. Iriyama, M. Suguro and E. Hasegawa, *Chem. Phys. Lett.*, 2002, **359**, 351–354.
8 K. Zhang, Y. Hu, L. Wang, J. Fan, M. J. Monteiro and Z. Jia, *Polym. Chem.*, 2017, **8**, 1815–1823.
9 K. Oyaizu, Y. Ando, H. Konishi and H. Nishide, *J. Am. Chem. Soc.*, 2008, **130**, 14459–14461.
10 C. Luo, O. Borodin, X. Ji, S. Hou, K. J. Gaskell, X. Fan, J. Chen, T. Deng, R. Wang, J. Jiang and C. Wang, *Proc. Natl. Acad. Sci. U. S. A.*, 2018, **115**, 2004–2009.
11 C. Luo, X. Ji, S. Hou, N. Eidson, X. Fan, Y. Liang, T. Deng, J. Jiang and C. Wang, *Adv. Mater.*, 2018, **30**, 1706498.
12 S. Zhang, F. Xing, L. Chen, X. Wang and X. He, *Chem. Mater.*, 2022, **34**, 9031–9041.
13 H.-g. Wang, S. Yuan, D.-l. Ma, X.-l. Huang, F.-l. Meng and X.-b. Zhang, *Adv. Energy Mater.*, 2014, **4**, 1301651.
14 F. Xing, S. Li, L. Chen, J.-S. Dang and X. He, *ACS Nano*, 2023, **17**, 21432–21442.
15 L. Zhu, G. Ding, L. Xie, X. Cao, J. Liu, X. Lei and J. Ma, *Chem. Mater.*, 2019, **31**, 8582–8612.
16 W. Choi, D. Harada, K. Oyaizu and H. Nishide, *J. Am. Chem. Soc.*, 2011, **133**, 19839–19843.
17 Z. Song, Y. Qian, M. L. Gordin, D. Tang, T. Xu, M. Otani, H. Zhan, H. Zhou and D. Wang, *Angew. Chem., Int. Ed.*, 2015, **54**, 13947–13951.
18 Z. Song, Y. Qian, T. Zhang, M. Otani and H. Zhou, *Adv. Sci.*, 2015, **2**, 1500124.
19 X. He, L. Chen and T. Baumgartner, *ACS Appl. Mater. Interfaces*, 2023, DOI: **10.1021/acsami.3c09856**.
20 M. Stolar, C. Reus and T. Baumgartner, *Adv. Energy Mater.*, 2016, **6**, 1600944.
21 T. Ma, L. Liu, J. Wang, Y. Lu and J. Chen, *Angew. Chem., Int. Ed.*, 2020, **59**, 11533–11539.
22 L. Chen, X. Zhu, Y. Zhang, G. Gao, W. Xue, S. Zhang, X. Wang, Q. Zhang and X. He, *J. Mater. Chem. A*, 2021, **9**, 18506–18514.
23 Z. Wang, A. Duan, W. Jin, X. Huang and Y. Li, *J. Mater. Chem. A*, 2022, **10**, 10026–10032.

24 C. Peng, G.-H. Ning, J. Su, G. Zhong, W. Tang, B. Tian, C. Su, D. Yu, L. Zu, J. Yang, M.-F. Ng, Y.-S. Hu, Y. Yang, M. Armand and K. P. Loh, *Nat. Energy*, 2017, **2**, 17074.
25 J. Huang, S. Hu, X. Yuan, Z. Xiang, M. Huang, K. Wan, J. Piao, Z. Fu and Z. Liang, *Angew. Chem., Int. Ed.*, 2021, **60**, 20921–20925.
26 J. Shukla, M. R. Ajayakumar, Y. Kumar and P. Mukhopadhyay, *Chem. Commun.*, 2018, **54**, 900–903.
27 B. Lee, Y. Ko, G. Kwon, S. Lee, K. Ku, J. Kim and K. Kang, *Joule*, 2018, **2**, 61–75.
28 T. B. Schon, A. J. Tilley, C. R. Bridges, M. B. Miltenburg and D. S. Seferos, *Adv. Funct. Mater.*, 2016, **26**, 6896–6903.
29 G. Gao, X. Wang, L. Chen, T. Baumgartner and X. He, *Chem. Mater.*, 2021, **33**, 4596–4605.
30 X. Wang, W. Xue, G. Gao, L. Chen, T. Baumgartner and X. He, *Cell Rep. Phys. Sci.*, 2022, **3**, 100951.
31 Q. T. Lin, H. Y. Li, L. Chen and X. He, *Mater. Chem. Front.*, 2023, **7**, 3747–3753.
32 F. Wang, J. Wang, G. Li, Z. Guo, J. Chu, X. Ai and Z. Song, *Energy Storage Mater.*, 2022, **50**, 658–667.
33 F. Otteny, M. Kolek, J. Becking, M. Winter, P. Bieker and B. Esser, *Adv. Energy Mater.*, 2018, **8**, 1802151.
34 S. Banfi, L. Carlucci, E. Caruso, G. Ciani and D. M. Proserpio, *Dalton Trans.*, 2002, 2714–2721.
35 Q. Sui, P. Li, R. Sun, Y.-H. Fang, L. Wang, B.-W. Wang, E.-Q. Gao and S. Gao, *J. Phys. Chem. Lett.*, 2020, **11**, 9282–9288.
36 A. J. Bard and L. R. Faulkner, *Electrochemical Methods: Fundamentals and Applications*, 2nd edn, Wiley, New York, 2001.
37 M. Pan, Y. Lu, S. Lu, B. Yu, J. Wei, Y. Liu and Z. Jin, *ACS Appl. Mater. Interfaces*, 2021, **13**, 44174–44183.
38 J. Luo, B. Hu, C. Debruler and T. L. Liu, *Angew. Chem., Int. Ed.*, 2018, **57**, 231–235.
39 L. Lin, Z. Lin, J. Zhu, K. Wang, W. Wu, T. Qiu and X. Sun, *Energy Environ. Sci.*, 2023, **16**, 89–96.
40 G. Dai, Y. Liu, Z. Niu, P. He, Y. Zhao, X. Zhang and H. Zhou, *Matter*, 2019, **1**, 945–958.
41 S. Xu, H. Li, Y. Chen, Y. Wu, C. Jiang, E. Wang and C. Wang, *J. Mater. Chem. A*, 2020, **8**, 23851–23856.
42 Y. Liu, Z. Niu, G. Dai, Y. Chen, H. Li, L. Huang, X. Zhang, Y. Xu and Y. Zhao, *Mater. Today Energy*, 2021, **21**, 100812.
43 V. Augustyn, J. Come, M. A. Lowe, J. W. Kim, P.-L. Taberna, S. H. Tolbert, H. D. Abruña, P. Simon and B. Dunn, *Nat. Mater.*, 2013, **12**, 518–522.
44 H. Lindström, S. Södergren, A. Solbrand, H. Rensmo, J. Hjelm, A. Hagfeldt and S.-E. Lindquist, *J. Phys. Chem. B*, 1997, **101**, 7717–7722.